Size-Resolved Photoelectron Anisotropy of Gas Phase Water Clusters and Predictions for Liquid Water

Sebastian Hartweg,[1] Bruce L. Yoder,[1] Gustavo A. Garcia,[2] Laurent Nahon,[2] and Ruth Signorell[1,*]
[1]Department of Chemistry and Applied Biosciences, Laboratory of Physical Chemistry, ETH Zürich, Vladimir-Prelog-Weg 2, CH-8093 Zürich, Switzerland
[2]Synchrotron SOLEIL, L'Orme des Merisiers, Saint Aubin BP 48, 91192 Gif sur Yvette, France
(Received 8 December 2016; published 10 March 2017)

We report the first measurements of size-resolved photoelectron angular distributions for the valence orbitals of neutral water clusters with up to 20 molecules. A systematic decrease of the photoelectron anisotropy is found for clusters with up to 5–6 molecules, and most remarkably, convergence of the anisotropy for larger clusters. We suggest the latter to be the result of a local short-range scattering potential that is fully described by a unit of 5–6 molecules. The cluster data and a detailed electron scattering model are used to predict the anisotropy of slow photoelectrons in liquid water. Reasonable agreement with experimental liquid jet data is found.

DOI: 10.1103/PhysRevLett.118.103402

A detailed understanding of elastic and inelastic scattering of electrons in liquid water is of fundamental importance for modeling radiation damage in biological systems, describing the behavior of the solvated electron in chemistry, and for the quantitative interpretation of photoelectron spectra of liquid water and aqueous solutions [1–8]. For slow electrons (electron kinetic energy eKE $\lesssim 50$ eV), detailed experimental scattering parameters (differential cross sections, energy losses) were only reported for *amorphous ice* [9]—apart from *liquid water* data for eKE $\lesssim 6$ eV recently obtained from photoelectron velocity map imaging (VMI) of water droplets [10]. As the energetics of electronic scattering processes (dissociative electron attachment, electronic excitations, ionization) are hardly affected by the finer details of the bulk environment, there is little reason to expect substantial differences between amorphous ice and liquid water for eKE $\gtrsim 6$ eV [9]. The amorphous ice and liquid droplet data [9,10] should thus provide a reasonable basis for scattering simulations of liquid water. In addition, electron attenuation lengths (EALs) for eKE $\gtrsim 3$ eV are available from various microjet studies [11–13]. The individual scattering contributions required for quantitative predictions can, however, not be extracted from EALs because EALs are broad averages over many different scattering processes.

As the photoelectron angular distribution (PAD) is particularly sensitive to electron scattering it has recently received increasing attention in this context [7,10,13–18]. It is often described by a single anisotropy parameter β, defined by

$$I(\theta) \propto 1 + \frac{\beta}{2}(3\cos^2\theta - 1). \quad (1)$$

θ is the angle between the light polarization and the ejection direction of the photoelectrons. $I(\theta)$ is the electron signal detected at that angle. For the liquid microjet, where the spherical symmetry of the sample is broken, this is an approximation, which we also use in the present work. For ionization from the O1s orbital of water, Thürmer *et al.* observed a more isotropic PAD (a smaller β value) for the liquid than for the gas phase in the eKE range ~12–450 eV [13]. For core-level ionization, this reduction should mainly arise from electron scattering within the liquid. For the ionization from the valence orbitals $1b_1$, $3a_1$, and $1b_2$, additional changes in the initial state due to orbital mixing, partly mediated by hydrogen bonding, are expected to contribute to differences in β between the gas and liquid phase. While monomer gas phase β parameters have been reported for the three valence orbitals at photon energies 18 eV $\leq h\nu <$ 139 eV [15,16,19–21], corresponding liquid water values have only been reported at $h\nu = 38.7$ eV [16]. Zhang *et al.* [15] made a first attempt to distinguish between initial state and scattering effects on β, based on measurements at $h\nu = 40$ and 60 eV of $(H_2O)_n$ clusters with broad size distributions and estimated average sizes of $\langle n \rangle \geq 58$. The results hinted at intrinsic differences between gas phase monomer and cluster PADs arising from alterations in the initial states. Table T1 in the Supplemental Material [22] summarizes the existing literature values for β parameters of water clusters and liquid water.

The present work reports double imaging photoelectron photoion coincidence i^{2}PEPICO measurements of small $(H_2O)_n$ clusters ($n \leq 20$) recorded at the synchrotron radiation facility SOLEIL, DESIRS beamline [22,28–32]. As a unique feature, this technique allows us to record photoelectron VMIs for a particular cluster size n. Avoiding averaging over different cluster sizes and circumventing the issue of the overlap with the strong water monomer signal we can extract cluster size-resolved β parameters. Size selectivity is particularly important for small clusters, where pronounced changes in β are expected for size changes by

just one water molecule. To clarify the evolution of PADs with increasing cluster size is our main goal. Clusters are not expected to be good models for the PAD of the liquid since most of the effects of elastic and inelastic scattering during electron transport in the bulk [referred to as contribution (iv) below] would be missing. Still, many local effects [referred to as contributions (i)–(iii)] can already be observed in clusters. As a link between the monomer and the condensed phase, clusters contribute to a better understanding of the complex electron scattering in liquid water. With this in mind, we predict β parameters for typical liquid water microjet experiments using a detailed scattering model [7,9,10,22]. We focus on slow electrons with eKEs ≤ 65 eV, where PADs sensitively depend on electron scattering.

Figure 1 shows β for the gas phase monomer ($n = 1$) in the range $13.0\ \text{eV} \leq h\nu \leq 35.0\ \text{eV}$ with corresponding values tabulated in Table T2 [22]. Figure S2 in Ref. [22] provides a comparison with published data for $h\nu \geq 18$ eV [15,16,19,20]. Our monomer data agree well with literature values and provide the first value below photon energies of ~18 eV, which clearly confirm the trend towards low anisotropies at very low eKEs (~0.4–5.4 eV) predicted by calculations [21]. Figure 1 also includes a summary of our experimental β parameters for $(H_2O)_n$ with $2 \leq n \leq 20$, recorded with i^{2}PEPICO (see Table T2 in Ref. [22] for corresponding values with respective uncertainties). For larger clusters at higher $h\nu$, some data points are missing because the signal to noise ratio was insufficient to determine reliable β parameters. Photoionization of a neutral water cluster $(H_2O)_n$ is accompanied by a fast intracluster proton transfer with subsequent loss of an OH radical [33–38]:

$$(H_2O)_n + h\nu = (H_2O)_{n-1}H^+ + OH + e^-. \qquad (2)$$

Accordingly, we assign clusters with n molecules to VMIs recorded in coincidence with mass $m = (n \times 18) - 17$. For small clusters the subsequent slow loss of water molecules from the initially formed protonated cluster is dominated by monomer loss with total decay fractions < 0.3 [33,34,40]. Figure 2 shows exemplary photoelectron spectra for $n = 1$, 2, and 6. In larger clusters polarization effects shift the vertical electron binding energy (VBE), i.e., the most probable electron binding energy (eBE), towards lower values (Fig. S4, [22]), although not yet reaching the liquid bulk value [41] or the values for large clusters [15,42]. The downward trend in cluster VBEs is consistent with the evolution of the cluster ion appearance energy from Ref. [33]. The dimer spectrum in Fig. 2(b) consists of the two contributions from the intact dimer $(H_2O)_2^+$ (red line) and from H_3O^+ (black line). Following Refs. [35,38], we attribute $(H_2O)_2^+$ to ionization from the lone pair of the hydrogen-bond donor [referred to as $(b_1)_D$], while H_3O^+ results from the ionization of an orbital delocalized over both hydrogen-bond donor and acceptor [referred to as (a_1/b_1)] with a clearly different β parameter [Fig. 1(a), brown crosses and full line, respectively]. Table T3 of the Supplemental Material [22] compares the corresponding dimer VBEs with literature data.

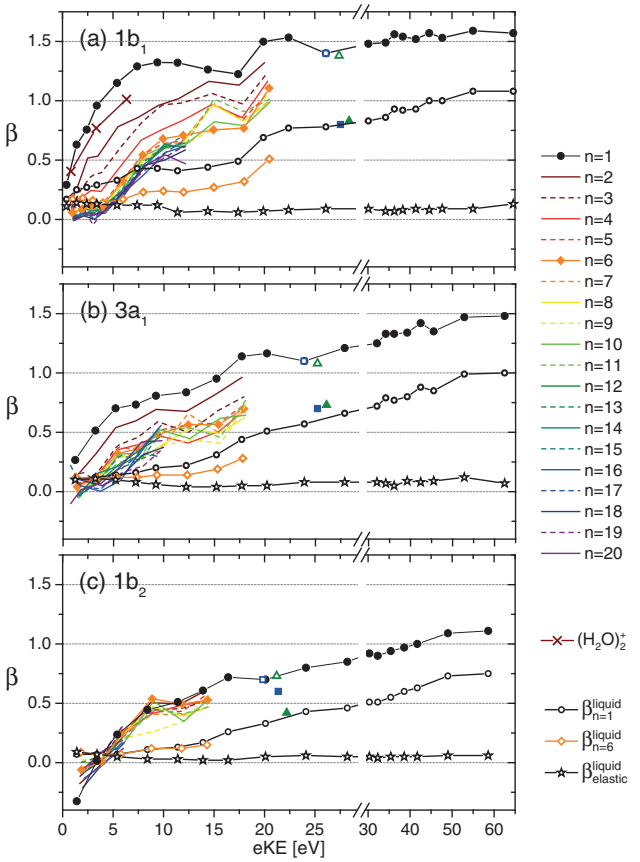

FIG. 1. Lines labeled $n = 1$ to $n = 20$: Experimental β parameters for H_2O monomer and $(H_2O)_n$ clusters with $2 \leq n \leq 20$ recorded at $13.0\ \text{eV} \leq h\nu \leq 35.0$ eV. (a),(b), and (c) correspond to ionization from the $1b_1$, $3a_1$, and $1b_2$ orbitals of water, respectively. Monomer values for eKEs < 25 eV from this work and for eKEs > 25 eV from Ref. [20]. For $(H_2O)_2$, separate traces are shown for H_3O^+ [full brown line; $n = 2$ Eq. (2)] and for the intact dimer $(H_2O)_2^+$ (brown crosses) [see Fig. 2(b)]. Green triangles: monomer (open symbols) and a cluster ensemble (full symbols) with an average cluster size $\langle n \rangle \sim 58$ from Ref. [15]. Blue squares: monomer (open symbols) and liquid water (full symbols) from the microjet study by Faubel *et al.* [16]. Calculated anisotropy parameters for liquid water microjets: Open black circles: $\beta_{n=1}^{\text{liquid}}$ calculated with monomer values ($n = 1$) as input for the local anisotropy in the liquid. Open orange diamonds: $\beta_{n=6}^{\text{liquid}}$ calculated with the cluster values ($n = 6$) as input for the local anisotropy in the liquid. Open black stars: $\beta_{\text{elastic}}^{\text{liquid}}$ calculated with gas phase elastic scattering cross sections alone [39].

Figure 1 provides the first quantitative β values for the initial condensation steps ($n = 2$–20). The largest absolute decrease of the anisotropy with increasing cluster size is observed for the $1b_1$ orbital (out-of-plane lone pair), followed by the $3a_1$ orbital (in-plane lone pair). The $1b_2$ orbital (σ_{OH} bond orbital) shows the smallest variations in β,

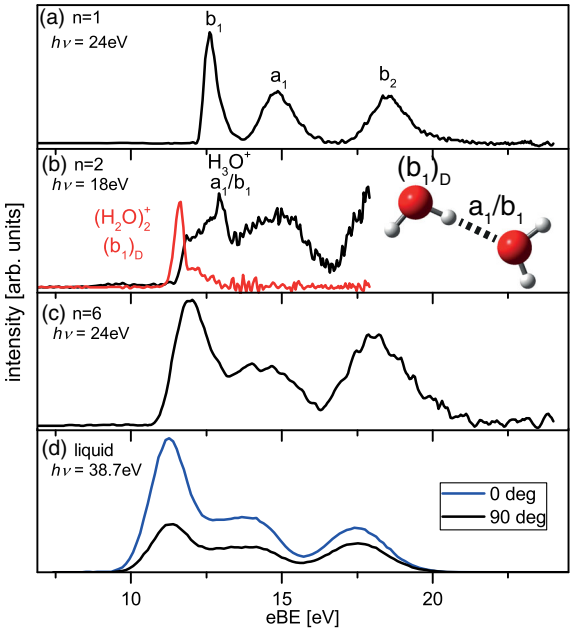

FIG. 2. Experimental photoelectron spectra of (a) water monomer and $(H_2O)_n$ clusters for (b) $n = 2$ and (c) $n = 6$. Selected VMI images are shown in Fig. S3 of the Supplemental Material [22]. The dimer spectrum has contributions from the intact dimer $(H_2O)_2^+$ (red line) and from H_3O^+ (black line) formed after fast proton transfer. (d) Calculated photoelectron spectra for the liquid water microjet for two polarization directions $\theta = 0°$ (blue line) and 90° (black line) of the light (Fig. S5, [22]) for monomer input $\beta_{n=1}$ (Fig. 1). The photon energies $h\nu$ are indicated in the figure.

but within the estimated uncertainty no systematic trend with cluster size. The larger sensitivity of β for ionization from $1b_1$ compared with $1b_2$ seems reasonable because the $1b_1$ orbital acts as an acceptor in hydrogen bonds, while $1b_2$ (σ_{OH}) is not directly involved in hydrogen bonding. Similar trends compared with the monomer were observed for the cluster ensemble at 40 eV [15] and the liquid microjet at 38.7 eV [16]. The most striking result in Fig. 1 is the convergence of β for the two outermost valence orbitals for cluster sizes $n \gtrsim 5$–6. A simple estimate based on the maximum number of monomers that can evaporate from a cluster after proton transfer and the reported cluster decay rates shows that the slow cluster evaporation does not significantly affect the β value derived for a given cluster size [33,34,40] and thus cannot explain the observed convergence.

We suggest the following qualitative explanation for the systematic decrease of $|\beta|$ with increasing n and its convergence for $n \gtrsim 5$–6. (Note that for larger clusters the observed β is the average over several conformers). The difference between molecular and cluster PADs arises from several contributions. (i) A change in the initial molecular electron wave function, i.e., a change in the local orbital character (polarization, orbital mixing) due to condensation. In $(H_2O)_n$ clusters, electron delocalization over hydrogen bonds is likely a major factor determining the change of orbital character. For increasing cluster size, changes in the orbital character typically reduce $|\beta|$. (ii) The second contribution is attributed to multicenter ionization—again a change in the initial state: The larger the cluster the more equivalent units are taking part in a single ionization event (quasidegeneracy). Interference of partial waves from many centers tends to reduce $|\beta|$, likely the more pronounced the larger the cluster. (iii) The third contribution comes from a change in the ion core potential, by which the outgoing electron wave is scattered. This is the result of the delocalization of the electron hole over nearest neighbors connected through hydrogen bonds, as discussed in detail for the case of the dimer in Ref. [35]. Again, this tends to reduce $|\beta|$. Qualitatively, all three contributions favor more isotropic PADs, i.e., a decrease of $|\beta|$, with increasing cluster size. This expectation agrees with the experimental observation for cluster sizes up to $n = 5$–6 (Fig. 1). The convergence of β observed for $n \gtrsim 5$–6 implies that the range of contributions (i)–(iii) only extends over a few molecules. $n \approx 5$–6 coincides with the smallest cluster sizes for which three-dimensional hydrogen-bond networks with more than two hydrogen bonds per water molecule become more stable than ring-topology structures (Refs. [43–46] and references therein). It is plausible that the typical range for changes in orbital character and in the ion core potential is comparable to the range of local hydrogen bridges. Similarly, interference effects from multicenter ionization should be most pronounced just in a local environment. The convergence of β for $6 \lesssim n \lesssim 20$ agrees with an intrinsic, short-range scattering potential that is described by a cluster with $n \approx 6$. Since the spatial extent of clusters with $n \lesssim 20$ is very small (~7–10 Å) the long-range scattering potential is essentially an unshielded Coulomb potential. Even semi-quantitative descriptions of the cluster PADs would require very high-level quantum chemical calculations [17,47–49]—still a big challenge for such complex systems.

In principle, the $|\beta|$ value of larger clusters could also be reduced by nonlocal elastic and inelastic scattering of the electrons during electron transport through the cluster, referred to as contribution (iv). We determine its influence by simulating cluster VMIs for different cluster sizes with our scattering model described in Sec. S3 of Ref. [22] and Ref. [10]. It is based on a Monte Carlo solution of the transport problem, equivalent to a random succession of suitably parametrized isolated scattering events. Our simulations explicitly take into account the cross sections, energetics, and angular dependences of all relevant scattering processes (inelastic electron-phonon, electron-vibron, electron-electron scattering, and elastic scattering). For $n \lesssim 50$ the influence of contribution (iv) is negligible (Fig. S7, [22]). A significant change of β (on the order of 0.1) is only found for clusters with more than $n \approx 100$ molecules, i.e., beyond cluster sizes studied here. This also shows that previously used simple modeling approaches, such as gas phase scattering between the monomers in a cluster, are not suitable to describe the cluster behavior.

The water dimer is a special case because ionization from the lone pair of the hydrogen-bond donor $(b_1)_D$ is distinguishable from ionization of the mixed (a_1/b_1) orbital, which is delocalized over donor and acceptor [Fig. 2(b)]. The β parameters for $(b_1)_D$ [brown crosses in Fig. 1(a)] are slightly lower than the monomer value ($n = 1$, full black circles). The $(b_1)_D$ orbital can be considered as a monomer orbital disturbed by the presence of the second H_2O molecule. As it is not directly involved in the hydrogen bond the decrease in β relative to the monomer mainly arises from contribution (i). The larger decrease of β for the (a_1/b_1) orbital ($n = 2$, full brown line) results from the simultaneous action of all three contributions (i)–(iii). It is unfortunately not possible to estimate the relative magnitude of (i) compared with (ii–iii) from the absolute changes of the two different dimer β parameters, but the general trend is consistent with our expectation that contributions (i)–(iii) tend to reduce $|\beta|$. When comparing absolute changes one must account for the fact that β is not proportional to the observed signal $I(\theta)$ [Eq. (1)].

In contrast to the clusters studied here, the liquid water PAD is not only determined by the three local contributions (i)–(iii), but also strongly by contribution (iv), i.e., elastic and inelastic scattering during electron transport in the liquid. We treat this effect within the detailed scattering model mentioned above (Sec. S3 in Ref. [22] and Refs. [7,9,10]) to simulate a typical liquid microjet experiment [12–14,16–18], illustrated in Fig. S5 of the Supplemental Material [22], where β^{liquid} is determined from polarization-dependent (θ-dependent) measurements. We assume the local contributions (i)–(iii) in liquid water to be either the same as in the monomer or the same as in a cluster with $n = 6$ (converged cluster value). Correspondingly we use either the experimental monomer ($\beta_{n=1}$; full black circles) or the experimental cluster ($\beta_{n=6}$; full orange diamonds) β parameters from Fig. 1 to describe the local anisotropies in the liquid. With the chosen local input anisotropy ($\beta_{n=1}$ or $\beta_{n=6}$) and our scattering model to account for contribution (iv) we calculate the liquid anisotropy parameters, $\beta^{\text{liquid}}_{n=1}$ (open black circles) and $\beta^{\text{liquid}}_{n=6}$ (open orange diamonds), respectively, shown in Fig. 1. The comparison with $\beta_{n=1}$ and $\beta_{n=6}$ illustrates the pronounced effect of contribution (iv) on the PADs of the liquid, viz. a reduction of the anisotropy. Figure 2(d) shows examples of photoelectron spectra of the liquid calculated for 0° and 90° laser polarization (see also Fig. S6 of Ref. [22]), which agree well with experimental liquid-jet spectra [16,41] (note the large gas phase fractions in the spectra of Ref. [16]). We finally note that polarization-dependent liquid jet measurements in principle yield marginally higher β values than other methods, such as VMI, because the coupling of the electromagnetic radiation into the jet depends on the laser polarization (Sec. S3, p. S9 of the Supplemental Material [22]).

To the best of our knowledge experimental values for β^{liquid} in the valence region were only reported at $h\nu = 38.7$ eV in a microjet study by Faubel *et al.* [16] (Fig. 1, full blue squares at eKEs ~ 21–28 eV). They lie reasonably close to our calculated β^{liquid} values in Fig. 1. The agreement is best for b_1, where monomer and liquid bands are well separated in the photoelectron spectrum [Figs. 2(a) and 2(d)]. The fact that for a_1 and b_2 the values of Faubel *et al.* lie above our calculations might be attributed to overlapping monomer bands not fully accounted for in the analysis of their experiment. Note the high β values of the monomer in the corresponding eKE range. In principle, our model should underestimate the true β^{liquid} because it does not account for the strong shielding of the ion core potential in the liquid, which is mainly dielectric screening. It reduces the range of the ion core potential by roughly an order of magnitude compared with the isolated monomer or cluster. Our simulations with input values $\beta_{n=1}$ and $\beta_{n=6}$ do not include this effect. A shorter range of the ion core potential reduces the influence of scattering by the ion core on the local anisotropy of the electron. This effect could be described by correspondingly higher input values for $\beta_{n=1}$ and $\beta_{n=6}$. This in turn would yield higher calculated β^{liquid} values. The apparent better agreement of the experimental data by Faubel *et al.* with $\beta^{\text{liquid}}_{n=1}$ than with $\beta^{\text{liquid}}_{n=6}$ appears to be fortuitous. Once dielectric screening is included, $\beta^{\text{liquid}}_{n=6}$ should actually agree better with experimental liquid bulk data, simply because the cluster input $\beta_{n=6}$ better represents the contributions (i)–(iii) as discussed above. A simple estimate of the influence of shielding is unfortunately not possible. Such estimates would require high-level *ab initio* calculations. In Fig. 1 we also add a calculation for the liquid anisotropy $\beta^{\text{liquid}}_{\text{elastic}}$ (open black stars), for which we used just elastic gas phase monomer scattering cross sections [39] instead of the proper condensed phase values as for the other simulations [9,10]. The resulting $\beta^{\text{liquid}}_{\text{elastic}}$ are almost isotropic and clearly disagree with the experimental values at $h\nu = 38.7$ eV. This demonstrates that gas phase scattering parameters are not suitable to describe the liquid.

In summary, photoelectron photoion concidence imaging provides size-dependent photoelectron anisotropy parameters of $(H_2O)_n$ clusters for $n \leq 20$. The experimental data suggest that intracluster electron scattering in clusters containing between ~6 and 20 molecules is mainly determined by the short range potential of a unit consisting of 5–6 molecules, coinciding with the smallest cluster sizes for which three-dimensional hydrogen-bond networks become the most stable structures. It seems reasonable that the short range scattering potential in liquid water is largely determined by this smallest unit; i.e., approximately by the first solvation shell. In contrast to clusters, however, the ion core potential is strongly shielded in the liquid. While a quantitative estimate of this effect can at present not be provided, it appears plausible that shielding will increase the anisotropy compared with the experimental

cluster data. We suspect that the major difference between small clusters ($n \lesssim 100$) and the liquid arises from the additional elastic and inelastic electron scattering in the liquid. A detailed scattering simulation for the liquid starting from cluster anisotropies of the smallest unit confirms this presumption. Even with the shielding effect neglected, this model provides reasonable agreement with experimental liquid jet data. Our simulations demonstrate that gas phase scattering parameters are generally not appropriate for electron scattering in the liquid. Further validation of the role of the smallest cluster unit and the shielding in the liquid awaits more experimental data from liquid jets and larger water clusters as well as in-depth theoretical studies.

We thank Dr. David Luckhaus for help with the calculations and David Stapfer and Markus Steger for technical support. We are grateful to the SOLEIL staff for smoothly running the facility under Project No. 20160122, particularly to Jean-François Gil and Duçan Bozanic for their technical support on the SAPHIRS experimental chamber. Financial support was provided by the ETH Zürich and the Swiss National Science Foundation under Project No. 200020_159205.

*Corresponding author.
rsignorell@ethz.ch

[1] E. Alizadeh, T. M. Orlando, and L. Sanche, Biomolecular damage induced by ionizing radiation: The direct and indirect effects of low-energy electrons on DNA, Annu. Rev. Phys. Chem. **66**, 379 (2015).
[2] B. Abel, Hydrated interfacial ions and electrons, Annu. Rev. Phys. Chem. **64**, 533 (2013).
[3] B. C. Garrett *et al.*, Role of water in electron-initiated processes and radical chemistry: Issues and scientific advances, Chem. Rev. **105**, 355 (2005).
[4] R. Seidel, B. Winter, and S. Bradforth, Valence electronic structure of aqueous solutions: Insights from photoelectron spectroscopy, Annu. Rev. Phys. Chem. **67**, 283 (2016).
[5] T. Suzuki, Time-resolved photoelectron spectroscopy of non-adiabatic electronic dynamics in gas and liquid phases, Int. Rev. Phys. Chem. **31**, 265 (2012).
[6] J. M. Herbert and M. P. Coons, The hydrated electron, Annu. Rev. Phys. Chem., DOI: 10.1146/annurev-physchem-052516-050816 (2017).
[7] D. Luckhaus, Y.-I. Yamamoto, T. Suzuki, and R. Signorell, Genuine Binding Energy of the Hydrated Electron, Sci. Adv. (to be published).
[8] R. M. Young and D. M. Neumark, Dynamics of solvated electrons in clusters, Chem. Rev. **112**, 5553 (2012).
[9] M. Michaud, A. Wen, and L. Sanche, Cross sections for low-energy (1–100 eV) electron elastic and inelastic scattering in amorphous ice, Radiat. Res. **159**, 3 (2003).
[10] R. Signorell, M. Goldmann, B. L. Yoder, A. Bodi, E. Chasovskikh, L. Lang, and D. Luckhaus, Nanofocusing, shadowing, and electron mean free path in the photoemission from aerosol droplets, Chem. Phys. Lett. **658**, 1 (2016).
[11] F. Buchner, T. Schultz, and A. Lübcke, Solvated electrons at the water-air interface: Surface versus bulk signal in low kinetic energy photoelectron spectroscopy, Phys. Chem. Chem. Phys. **14**, 5837 (2012).
[12] N. Ottosson, M. Faubel, S. E. Bradforth, P. Jungwirth, and B. Winter, Photoelectron spectroscopy of liquid water and aqueous solution: Electron effective attenuation lengths and emission-angle anisotropy, J. Electron Spectrosc. Relat. Phenom. **177**, 60 (2010).
[13] S. Thürmer, R. Seidel, M. Faubel, W. Eberhardt, J. C. Hemminger, S. E. Bradforth, and B. Winter, Photoelectron Angular Distributions from Liquid Water: Effects of Electron Scattering, Phys. Rev. Lett. **111**, 173005 (2013).
[14] Y.-I. Suzuki, K. Nishizawa, N. Kurahashi, and T. Suzuki, Effective attenuation length of an electron in liquid water between 10 and 600 eV, Phys. Rev. E **90**, 010302 (2014).
[15] C. Zhang, T. Andersson, M. Förstel, M. Mucke, T. Arion, M. Tchaplyguine, O. Björneholm, and U. Hergenhahn, The photoelectron angular distribution of water clusters, J. Chem. Phys. **138**, 234306 (2013).
[16] M. Faubel, K. R. Siefermann, Y. Liu, and B. Abel, Ultrafast soft X-ray photoelectron spectroscopy at liquid water microjets, Acc. Chem. Res. **45**, 120 (2012).
[17] Y.-I. Yamamoto, Y.-I. Suzuki, G. Tomasello, T. Horio, S. Karashima, R. Mitrić, and T. Suzuki, Time- and Angle-Resolved Photoemission Spectroscopy of Hydrated Electrons near a Liquid Water Surface, Phys. Rev. Lett. **112**, 187603 (2014).
[18] S. Karashima, Y. Yamamoto, and T. Suzuki, Resolving Nonadiabatic Dynamics of Hydrated Electrons Using Ultrafast Photoemission Anisotropy, Phys. Rev. Lett. **116**, 137601 (2016).
[19] C. M. Truesdale, S. Southworth, P. H. Kobrin, D. W. Lindle, G. Thornton, and D. A. Shirley, Photo-electron angular-distributions of H_2O, J. Chem. Phys. **76**, 860 (1982).
[20] M. S. Banna, B. H. McQuaide, R. Malutzki, and V. Schmidt, The photoelectron-spectrum of water in the 30–140 eV photon energy-range, J. Chem. Phys. **84**, 4739 (1986).
[21] M. V. Vega, C. Lavín, and A. M. Velasco, Angular distribution of photoelectrons in small molecules: A molecular quantum defect calculation, J. Chem. Phys. **136**, 214308 (2012).
[22] See Supplemental Material at http://link.aps.org/supplemental/10.1103/PhysRevLett.118.103402 for a description of the experimental setup and the scattering calculations, and additional figures and tables, which includes Refs. [23–27].
[23] H. Hayashi and N. Hiraoka, Accurate measurements of dielectric and optical functions of liquid water and liquid benzene in the VUV region (1–100 eV) using small-angle inelastic X-ray scattering, J. Phys. Chem. B **119**, 5609 (2015).
[24] FDTD solutions, from Lumerical Solutions Inc. (www.lumerical.com).
[25] M. Goldmann, J. Miguel-Sánchez, A. H. C. West, B. L. Yoder, and R. Signorell, Electron mean free path from angle-dependent photoelectron spectroscopy of aerosol particles, J. Chem. Phys. **142**, 224304 (2015).
[26] C. G. Elles, A. E. Jailaubekov, R. A. Crowell, and S. E. Bradforth, Excitation-energy dependence of the mechanism

for two-photon ionization of liquid H_2O and D_2O from 8.3 to 12.4 eV, J. Chem. Phys. **125**, 044515 (2006).

[27] J. V. Coe, A. D. Earhart, M. H. Cohen, G. J. Hoffman, H. W. Sarkas, and K. H. Bowen, Using cluster studies to approach the electronic structure of bulk water: Reassessing the vacuum level, conduction band edge, and band gap of water, J. Chem. Phys. **107**, 6023 (1997).

[28] X. F. Tang, G. A. Garcia, J. F. Gil, and L. Nahon, Vacuum upgrade and enhanced performances of the double imaging electron/ion coincidence end-station at the vacuum ultraviolet beamline DESIRS, Rev. Sci. Instrum. **86**, 123108 (2015).

[29] G. A. Garcia, B. K. C. de Miranda, M. Tia, S. Daly, and L. Nahon, DELICIOUS III: A multipurpose double imaging particle coincidence spectrometer for gas phase vacuum ultraviolet photodynamics studies, Rev. Sci. Instrum. **84**, 053112 (2013).

[30] L. Nahon, N. de Oliveira, G. A. Garcia, J.-F. Gil, B. Pilette, O. Marcouille, B. Lagarde, and F. Polack, Desirs: A state-of-the-art VUV beamline featuring high resolution and variable polarization for spectroscopy and dichroism at SOLEIL, J. Synchrotron Radiat. **19**, 508 (2012).

[31] B. L. Yoder, K. B. Bravaya, A. Bodi, A. H. C. West, B. Sztáray, and R. Signorell, Barrierless proton transfer across weak CH···O hydrogen bonds in dimethyl ether dimer, J. Chem. Phys. **142**, 114303 (2015).

[32] G. A. Garcia, L. Nahon, and I. Powis, Two-dimensional charged particle image inversion using a polar basis function expansion, Rev. Sci. Instrum. **75**, 4989 (2004).

[33] L. Belau, K. R. Wilson, S. R. Leone, and M. Ahmed, Vacuum ultraviolet (VUV) photoionization of small water clusters, J. Phys. Chem. A **111**, 10075 (2007).

[34] F. Dong, S. Heinbuch, J. J. Rocca, and E. R. Bernstein, Dynamics and fragmentation of Van der Waals clusters: $(H_2O)_n$,$(CH_3OH)_n$, and $(NH_3)_n$ upon ionization by a 26.5 eV soft X-ray laser, J. Chem. Phys. **124**, 224319 (2006).

[35] E. Kamarchik, O. Kostko, J. M. Bowman, M. Ahmed, and A. I. Krylov, Spectroscopic signatures of proton transfer dynamics in the water dimer cation, J. Chem. Phys. **132**, 194311 (2010).

[36] C. Y. Ng, D. J. Trevor, P. W. Tiedemann, S. T. Ceyer, P. L. Kronebusch, B. H. Mahan, and Y. T. Lee, Photoionization of dimeric polyatomic-molecules—proton affinities of H_2O and HF, J. Chem. Phys. **67**, 4235 (1977).

[37] A. Bodi, J. Csontos, M. Kállay, S. Borkar, and B. Sztáray, On the protonation of water, Chem. Sci. **5**, 3057 (2014).

[38] S. Tomoda, Y. Achiba, and K. Kimura, Photo-electron spectrum of the water dimer, Chem. Phys. Lett. **87**, 197 (1982).

[39] H. Cho, Y. S. Park, H. Tanaka, and S. J. Buckman, Measurements of elastic electron scattering by water vapour extended to backward angles, J. Phys. B **37**, 625 (2004).

[40] J. H. Litman, B. L. Yoder, B. Schläppi, and R. Signorell, Sodium-doping as a reference to study the influence of intracluster chemistry on the fragmentation of weakly-bound clusters upon vacuum ultraviolet photoionization, Phys. Chem. Chem. Phys. **15**, 940 (2013).

[41] B. Winter, R. Weber, W. Widdra, M. Dittmar, M. Faubel, and I. V. Hertel, Full valence band photoemission from liquid water using EUV synchrotron radiation, J. Phys. Chem. A **108**, 2625 (2004).

[42] O. Björneholm, F. Federmann, S. Kakar, and T. Möller, Between vapor and ice: Free water clusters studied by core level spectroscopy, J. Chem. Phys. **111**, 546 (1999).

[43] J. K. Gregory and D. C. Clary, Structure of water clusters. The contribution of many-body forces, monomer relaxation, and vibrational zero-point energy, J. Phys. Chem. **100**, 18014 (1996).

[44] C. J. Tainter and J. L. Skinner, The water hexamer: Three-body interactions, structures, energetics, and OH-stretch spectroscopy at finite temperature, J. Chem. Phys. **137**, 104304 (2012).

[45] R. J. Saykally and D. J. Wales, Pinning down the water hexamer, Science **336**, 814 (2012).

[46] C. Pérez, M. T. Muckle, D. P. Zaleski, N. A. Seifert, B. Temelso, G. C. Shields, Z. Kisiel, and B. H. Pate, Structures of cage, prism, and book isomers of water hexamer from broadband rotational spectroscopy, Science **336**, 897 (2012).

[47] C. M. Oana and A. I. Krylov, Cross sections and photoelectron angular distributions in photodetachment from negative ions using equation-of-motion coupled-cluster Dyson orbitals, J. Chem. Phys. **131**, 124114 (2009).

[48] S. Gozem, A. O. Gunina, T. Ichino, D. L. Osborn, J. F. Stanton, and A. I. Krylov, Photoelectron wave function in photoionization: Plane wave or Coulomb wave?, J. Phys. Chem. Lett. **6**, 4532 (2015).

[49] A. Humeniuk, M. Wohlgemuth, T. Suzuki, and R. Mitrić, Time-resolved photoelectron imaging spectra from non-adiabatic molecular dynamics simulations, J. Chem. Phys. **139**, 134104 (2013).